Spontaneous symmetry breaking in correlated wave functions

Ryui Kaneko,[1] Luca F. Tocchio,[2] Roser Valentí,[1] Federico Becca,[2] and Claudius Gros[1]
[1] *Institute for Theoretical Physics, University of Frankfurt, Max-von-Laue-Straße 1, D-60438 Frankfurt a.M., Germany*
[2] *Democritos National Simulation Center, Istituto Officina dei Materiali del CNR, and SISSA-International School for Advanced Studies, Via Bonomea 265, I-34136 Trieste, Italy*
(Dated: March 22, 2016)

We show that Jastrow-Slater wave functions, in which a density-density Jastrow factor is applied onto an uncorrelated fermionic state, may possess long-range order even when all symmetries are preserved in the wave function. This fact is mainly related to the presence of a sufficiently strong Jastrow term (also including the case of full Gutzwiller projection, suitable for describing spin models). Selected examples are reported, including the spawning of Néel order and dimerization in spin systems, and the stabilization of charge and orbital order in itinerant electronic systems.

PACS numbers: 71.27.+a, 71.10.Fd, 75.10.-b, 75.10.Jm

arXiv:1510.08653v2 [cond-mat.str-el] 20 Mar 2016

I. INTRODUCTION

Exact ground-state wave functions are known only for a limited number of many-body Hamiltonians (with exact solutions for the entire spectrum being even rarer)[1]. Variational states provide, alternatively, educated guesses for the ground state and for low-energy excitations. As they are not related to particular weak-coupling approximations, variational approaches allow one to investigate nonperturbative effects. Nevertheless, they rely on an initial guess and may therefore sometimes be biased. Well-known examples of variational states are given by the Bardeen-Cooper-Schrieffer (BCS)[2] and Laughlin[3] wave functions, describing, respectively, conventional superconductivity and the fractional quantum Hall effect. Variational states have also been widely used ever since Gutzwiller's seminal work on the Hubbard model[4] in the context of correlated electronic and bosonic systems. A few benchmarking studies with other available many-body computational methods have been performed recently in the framework of the fermionic Hubbard model[5,6].

Within the variational approach, it is easy to describe quantum phase transitions. Usually, this is achieved by considering Hartree-Fock states, which contain a suitable order parameter, whose finite value indicates the stabilization of a symmetry-broken phase. One simple example is given by the half-filled Hubbard model on the honeycomb lattice, where antiferromagnetic order develops when the ratio between the on-site Coulomb interaction U and the nearest-neighbor hopping t exceeds a critical value[7]. Most importantly, within the Hartree-Fock approach, the presence of long-range order is obtained from an initial guess of the ordered pattern that is included into the wave function, thus implying an *explicit* symmetry breaking.

In this paper, we want to assess the possibility that symmetry-broken phases can be obtained by using *symmetry-invariant* wave functions, which implies that long-range order is obtained as a true spontaneous symmetry-breaking phenomenon. Even though no *explicit* bias is included in the wave functions, one must keep in mind that this approach cannot provide a completely unbiased way of obtaining *any* possible pattern for spin and/or charge order. We will show examples in which relatively simple orders emerge in symmetric states, while it remains a very hard task to devise a scheme in which a given wave function may describe many different spin and/or charge patterns that can be selected by tuning a few (variational) parameters.

In the context of spontaneous symmetry breaking, a well-known example is given by the Liang, Doucot, and Anderson (LDA) wave function, which was proposed to investigate quantum magnetism in the Heisenberg model on a square lattice[8]. The LDA state is written in terms of *bosonic* degrees of freedom (e.g., singlets that cover the entire lattice), and it embodies a possible representation of the resonating-valence-bond (RVB) states[9]. The LDA wave function is fully characterized by the weight factor $h(r)$ for a singlet of length r. To evaluate any expectation value over the LDA wave function, one must devise a stochastic sampling, based upon the Monte Carlo technique. Indeed, given the exponential increase of the dimension of Hilbert space, an exact treatment can be afforded only on very small clusters. Even though the LDA wave function does not break spin and lattice symmetries, it may describe magnetically ordered phases. This is the case when $h(r)$ decays slowly with r [e.g., $h(r) \propto 1/r^p$, with $p < 3.4$ on the square lattice]; by contrast, if $h(r)$ decays rapidly with r (e.g., $p > 3.4$), then the LDA wave function is magnetically disordered[8,10]. The great limitation of this wave function is that efficient Monte Carlo calculations can be afforded only in the presence of the Marshall sign rule[11]. In the absence of this rule, such as for triangular and kagome lattices, calculations suffer from a severe sign problem and only small cluster sizes can be afforded[12]. Therefore, its properties are well established in only a few cases.

Here, we consider an alternative approach and assess the possibility of having spontaneous symmetry breaking in a different family of quantum states, which are constructed from *fermionic* degrees of freedom, suitable to

describe both itinerant (i.e., Hubbard) and localized (i.e., Heisenberg) systems. In the latter case, these fermionic wave functions give rise to alternative representations of RVB states[9]. Moreover, dealing with fermions has the notable advantage that Monte Carlo calculations can be easily performed on large clusters and any lattice geometry. The simplest of this class of variational states is the well-known Gutzwiller wave function that was introduced to deal with correlated electron systems[4]:

$$|\Psi_g\rangle = \mathcal{P}_g|\Phi\rangle, \tag{1}$$

where $|\Phi\rangle$ is a noninteracting fermionic state that is obtained by filling N given orbitals labeled by some index γ (so that $|\Phi\rangle$ is an N-electron state):

$$|\Phi\rangle = \prod_{\gamma=1}^{N} \phi_\gamma^\dagger |0\rangle. \tag{2}$$

In practice, $|\Phi\rangle$ can be obtained as an eigenstate (usually the ground state) of a noninteracting Hamiltonian, containing, for example, hopping and pairing terms (in the presence of pairing between up and down electrons, one can always perform a particle-hole transformation to have a Hamiltonian that commutes with the particle number, thus defining "orbitals"). Finally, $\mathcal{P}_g$ is the so-called Gutzwiller factor, which depends upon the variational parameter g:

$$\mathcal{P}_g = \exp\left(-g\sum_i n_{i,\uparrow}n_{i,\downarrow}\right), \tag{3}$$

where $n_{i,\sigma}$ is the electron density per spin σ on the site i. The role of this term is to reduce the amplitudes of electron configurations with doubly occupied sites, thus tuning the level of electron correlation: $g = 0$ corresponds to noninteracting particles, while $g = \infty$ totally projects out configurations with doubly occupied sites, hence corresponding to the strongest possible electron-electron interaction. We would like to remind the reader that, also for fermionic wave functions such as the one given in Eq. (1), a Monte Carlo sampling is necessary to evaluate any expectation value for large system sizes. Indeed, in the presence of any correlation term, such as the Gutzwiller factor, analytical calculations are not possible in lattices of generic dimensionality.

In the following, N and L denote the number of electrons and lattice sites, respectively; $n = N/L$ is the electron density. By restricting to fully symmetric $|\Phi\rangle$, the correlated wave function (1) may describe metallic or superconducting phases for generic densities n; insulating phases are possible only at half-filling $n = 1$ and in the presence of a full Gutzwiller projector $g = \infty$[13,14]:

$$\mathcal{P}_\infty = \prod_i \left(1 - n_{i,\uparrow}n_{i,\downarrow}\right). \tag{4}$$

The is because the Gutzwiller term only correlates electrons on the same site: once charge excitations (holon-doublon couples) are created, the holon and the doublon are free to move around without any further penalization, thus leading to nonzero conductivity.

When $g = \infty$ and $n = 1$, charge degrees of freedom are completely frozen (i.e., there is exactly one electron on each site) and an insulator is obtained. Nevertheless, the fully projected state:

$$|\Psi\rangle = \mathcal{P}_\infty|\Phi\rangle \tag{5}$$

still contains nontrivial spin degrees of freedom, so that it can be used to study Heisenberg models[15].

A generalization of the Gutzwiller wave function (1) can be obtained by including density-density correlations at different sites, and it is given by the Jastrow-Slater state:

$$|\Psi_J\rangle = \mathcal{J}|\Phi\rangle, \tag{6}$$

where the Jastrow term includes correlations on different sites:

$$\mathcal{J} = \exp\left(-\frac{1}{2}\sum_{i,j} v_{i,j}n_i n_j\right); \tag{7}$$

here $v_{i,j}$ is a pseudo-potential for density fluctuations (the on-site term $v_{i,i}$ corresponds to the Gutzwiller parameter g) and $n_i = \sum_\sigma n_{i,\sigma}$ is the total density on site i. While long-range density-density correlations are crucial to describe a pure Mott insulator[16], here we will consider very simple Jastrow factors including only on-site and nearest-neighbor terms. In fact, already with this simple form, it is possible to describe situations in which symmetry-broken phases appear. Of course, long-range terms would be necessary also when considering more complicated charge/spin patterns.

The generalization to multi-orbital models is also straightforward: one should add orbital degrees of freedom in the noninteracting state $|\Phi\rangle$ (i.e., consider a noninteracting Hamiltonian with more than one orbital per site) and introduce a Jastrow factor that couples density fluctuations on different sites and orbitals:

$$\mathcal{J} = \exp\left(-\frac{1}{2}\sum_{i,j,\alpha,\beta} v_{i,j}^{\alpha,\beta} n_i^\alpha n_j^\beta\right), \tag{8}$$

where $v_{i,j}^{\alpha,\beta}$ is a pseudo-potential for density fluctuations ($v_{i,i}^{\alpha,\alpha} = g$, while $v_{i,i}^{\alpha,\beta}$ with $\alpha \neq \beta$ is the inter-orbital Gutzwiller parameter) and $n_i^\alpha = \sum_\sigma n_{i,\sigma}^\alpha$ is the charge density on the orbital α at site i.

We will show that different kinds of spontaneous symmetry-breaking phenomena are possible within Jastrow-Slater wave functions, i.e., when using Eq. (6): more precisely, even when both the noninteracting state $|\Phi\rangle$ and the Jastrow factor $\mathcal{J}$ preserve all the lattice and spin symmetries, clear signatures of order can be obtained. For example, in the case of a discrete symmetry breaking, e.g., charge order, clear evidence of ergodicity

breaking is detected when using single-particle moves in the Monte Carlo calculations. The use of fully symmetric wave functions allows us to describe quantum phase transitions by varying one parameter inside the variational wave function; for example, charge-density order is obtained in a system of itinerant electrons for a sufficiently strong nearest-neighbor Jastrow pseudo-potential (e.g., the one-dimensional lattice with $n = 1/2$ filling and the triangular lattice with $n = 2/3$ filling). These results can be understood thanks to a simple mapping from quantum averages to a *classical* problem of interacting particles. Then, the presence of a quantum phase transition when changing the variational state is directly connected to the existence of a classical phase transition in the related classical model.

In addition, we will also report the presence of antiferromagnetic long-range order in spin models, i.e., when using Eq. (5), similarly to what has been shown by using the LDA wave function. In this case, although the magnetization is exactly zero for all finite sizes (the quantum state is a spin singlet), magnetic order can be obtained in two dimensions whenever a suitable parametrization is considered. Furthermore, we will show that, within this class of fermionic states, the correct behavior is obtained in one dimension, namely spontaneous breaking of SU(2) symmetry does not occur, in agreement with the Mermin-Wagner theorem[17] and in contrast to bosonic states[18]. Instead, in one dimension, fermionic states may describe both gapless and dimerized (gapped) states, in agreement with the Lieb-Schultz-Mattis theorem[19].

The paper is organized as follows: In Sec. II, we show the results for the appearance of charge order for itinerant electrons in one spatial dimension and in the triangular lattice, as well as the emergence of orbital order in a two-band model on the square lattice; we will also see that the emergence of charge order can be understood by mapping the wave function into the classical counterpart. In Sec. III, we present the results for magnetization and dimerization by applying the fully projected wave function where the classical mapping is no longer available; we first show that the wave functions reproduce the correct behaviors in one-dimensional spin models, and then we examine how magnetic order appears in two-dimensional spin models. Finally, in Sec. IV we draw our conclusions.

II. CHARGE-DENSITY AND ORBITAL ORDER

A. The classical mapping

Certainly, charge order can be obtained when using a Jastrow factor or a Slater determinant that breaks translational invariance[20–22]. However, this is an expected outcome, which will not be treated here; instead, as discussed above, we are interested in the more subtle case in which charge (or orbital) order may be settled in a perfectly symmetry-invariant variational state.

The variational calculation with the wave function (6) can be shown to correspond to a classical problem at finite temperature[23–25]. This correspondence is very useful for showing that quantum phase transitions are possible within this class of variational states. To prove the mapping, let us consider a basis set $|x\rangle$ in which particles have definite positions in the lattice. For all operators θ that are diagonal in this basis, the quantum average:

$$\langle\theta\rangle = \frac{\langle\Psi|\theta|\Psi\rangle}{\langle\Psi|\Psi\rangle} \tag{9}$$

can be written in terms of the *classical* distribution:

$$\langle\theta\rangle = \sum_x P(x)\langle x|\theta|x\rangle, \tag{10}$$

where $P(x)$ is given by:

$$P(x) = \frac{|\langle x|\Psi\rangle|^2}{\langle\Psi|\Psi\rangle}. \tag{11}$$

Since $P(x) \geq 0$, there is a precise correspondence between the wave function and an effective classical potential $V_{\rm cl}(x)$:

$$P(x) \equiv \frac{1}{\mathcal{Z}} e^{-\beta_{\rm cl} V_{\rm cl}(x)}, \tag{12}$$

where $T_{\rm cl} = 1/\beta_{\rm cl}$ represents an effective classical temperature. The explicit form of the potential $V_{\rm cl}(x)$ depends upon the choice of the Jastrow factor and the form of the noninteracting state $|\Phi\rangle$:

$$\beta_{\rm cl} V_{\rm cl}(x) = \sum_{i,j} v_{i,j} n_i(x) n_j(x) - 2\ln\det\Phi(x), \tag{13}$$

where $n_i(x)$ is the electron density at site i for the configuration $|x\rangle$, i.e., $n_i|x\rangle = n_i(x)|x\rangle$ and $\Phi(x) = \langle x|\Phi\rangle$ is the amplitude of the noninteracting state over the configuration $|x\rangle$[23,24]. The first term of Eq. (13) is a two-body potential, which describes a classical model of oppositely charged particles (holons and doublons) mutually interacting through a given potential. In the presence of the second term in Eq. (13), $V_{\rm cl}(x)$ is no longer a two-body potential. However, when density fluctuations are suppressed (by the Gutzwiller factor), the quadratic term gives the most relevant contribution, hence the mapping onto a classical model of interacting particles still holds with $\beta_{\rm cl} V_{\rm cl}(x) \simeq \sum_{i,j} v_{i,j}^{\rm eff} n_i(x) n_j(x)$.

In the following, in order to detect charge-density order, we compute the density-density structure factor (that is a diagonal operator in the $|x\rangle$ basis):

$$N(q) = \frac{1}{L}\sum_{i,j}\langle n_i n_j\rangle e^{iq(r_i - r_j)}. \tag{14}$$

When order is present with a given periodicity Q, then $N(Q)/L$ is finite in the thermodynamic limit. Similarly, orbital order can be detected by considering, for example, the density-density correlations of the same orbital on different sites:

$$N^\alpha(q) = \frac{1}{L}\sum_{i,j}\langle n_i^\alpha n_j^\alpha\rangle e^{iq(r_i - r_j)}. \tag{15}$$

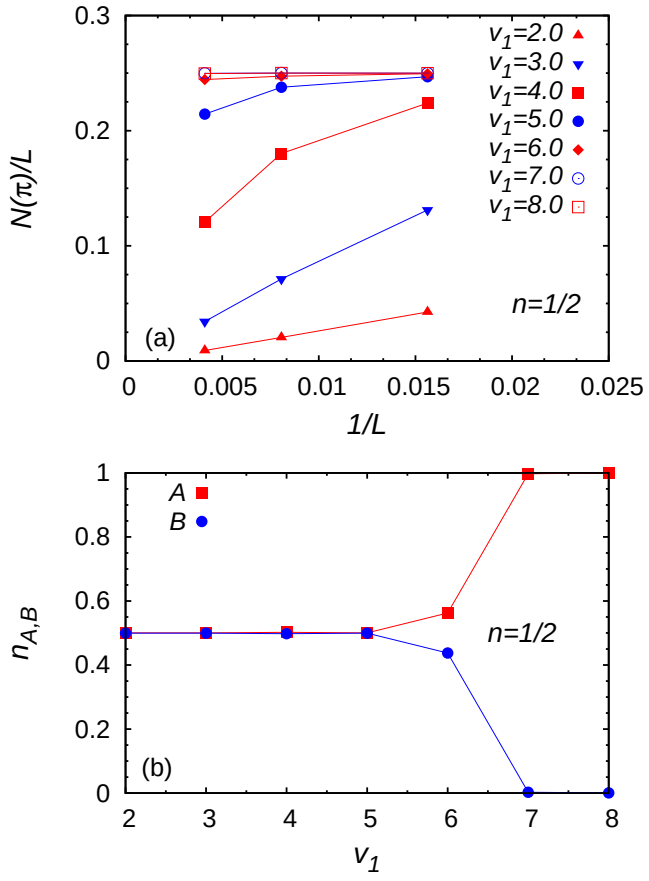

FIG. 1: (Color online) (a) Size scaling of $N(Q)/L$ at $Q = \pi$ for the one-dimensional case at quarter filling $n = 1/2$. The variational wave function is given by Eqs. (16) and (17) with $g = 10$ and different values of v_1. (b) Densities of the two sublattices A and B for the one-dimensional system at quarter filling $n = 1/2$ as a function of the Jastrow parameter v_1 (with $g = 10$) for $L = 244$ sites.

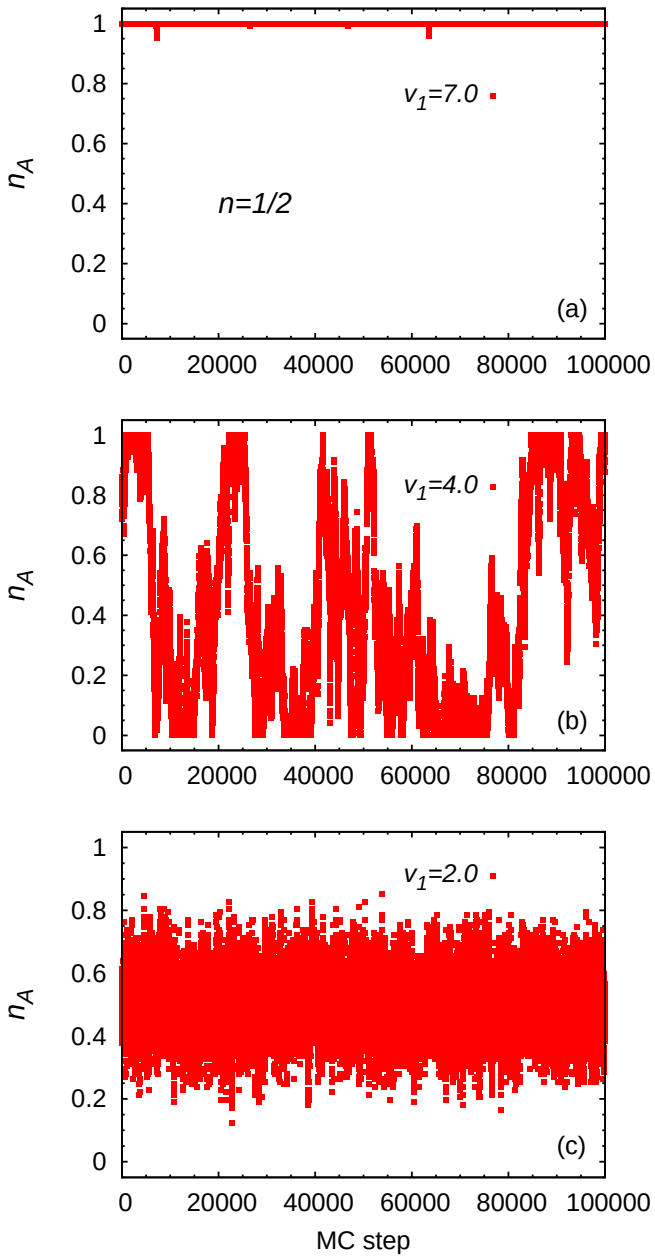

FIG. 2: (Color online) Monte Carlo evolution of the charge density on one sublattice for the one-dimensional system and $n = 1/2$ for $L = 244$ sites. Three different values of the Jastrow pseudo-potential v_1 are shown for the wave function described by Eqs. (16) and (17). $v_1 = 7.0$ (a), $v_1 = 4.0$ (b), $v_1 = 2.0$ (c).

B. Charge-density order in one dimension

Let us start by considering a one-dimensional system at quarter filling, i.e., $n = 1/2$. We analyze the properties of the Jastrow-Slater wave function in which the noninteracting state is given by filling the lowest-energy levels of free fermions having $\epsilon(k) = -2\cos k$:

$$|\Phi\rangle = \prod_{k<k_F,\sigma} c^\dagger_{k,\sigma}|0\rangle, \qquad (16)$$

where $k_F = \pi/4$ for quarter filling. In order to have a unique state, we consider chains with $L = 8l + 4$ sites, with l integer, and periodic boundary conditions. In addition, we take a simple Jastrow term that only contains on-site and nearest-neighbor pseudo-potentials:

$$\mathcal{J} = \exp\left(-g\sum_i n_{i,\uparrow}n_{i,\downarrow} - v_1\sum_i n_i n_{i+1}\right), \qquad (17)$$

where we fix $g = 10$ and vary v_1. Both the noninteracting state $|\Phi\rangle$ and the Jastrow term $\mathcal{J}$ are clearly invariant under translation and inversion symmetries. Nevertheless, the correlated wave function $|\Psi_J\rangle$ may describe two distinct phases for $n = 1/2$: for small values of v_1, the density is uniform in the lattice (the quantum state is metallic), while for large values of v_1 there is a 1−0−1−0 density order (corresponding to a charge-density-wave in-

sulator). We would like to mention that the variational wave function defined by Eqs. (16) and (17) is suitable for the extended Hubbard Hamiltonian that includes both on-site and nearest-neighbor interactions[26–31]:

$$\mathcal{H} = - t \sum_{i,\sigma} c^{\dagger}_{i,\sigma} c_{i+1,\sigma} + \text{h.c.} + U \sum_{i} n_{i,\uparrow} n_{i,\downarrow} + V \sum_{i} n_i n_{i+1}. \quad (18)$$

The existence of a phase transition when changing v_1 can be understood from the classical mapping. When v_1 is large, the first term of the r.h.s. of Eq. (13) dominates and drives the system into an ordered phase (this is expected from the classical model with nearest-neighbor interactions at low enough temperatures); by contrast, when v_1 is small, the first term of the r.h.s. of Eq. (13) does not give rise to charge-density order (i.e., the classical temperature is large). Notice that in this reasoning we assume that the contribution from the Slater determinant, i.e., the second term of the r.h.s. of Eq. (13), is not able to produce any transition, as expected for the chosen noninteracting part of Eq. (16).

At quarter filling, the density-density structure factor (14) computed over the correlated wave function shows a peak at $Q = \pi$, which behaves differently for small and large values of the parameter v_1. In Fig. 1(a), we report the size scaling of $N(Q)/L$ at $Q = \pi$ for different values of v_1. Here, a drastic change can be seen when varying v_1: for $v_1 \lesssim 5$ there is no charge-density order, i.e., $N(Q)/L$ goes to zero in the thermodynamic limit, while for $v_1 \gtrsim 5$ there is a clear evidence of order, $N(Q)/L$ being finite. For $v_1 \simeq 5$ considerable size effects are present, as expected close to a phase transition. The averaged values of the densities in the two sublattices A and B, $n_{A(B)} = 2/L \sum_{i \in A(B)} n_i$, as a function of v_1, are reported in Fig. 1(b).

It is important to notice that a breaking of the ergodicity (when using single-electron updates in the Monte Carlo sampling) is manifest when $v_1 \gtrsim 5$: while for small values of v_1 ergodicity is clearly obtained, for large v_1 ergodicity is broken and the simulation remains trapped into one of the possible degenerate (global) minima, with specific charge patterns. In Fig. 2, we report the evolution of the averaged charge density on one sublattice, as a function of Monte Carlo updating, for three values of v_1. While for $v_1 = 2$ [see Fig. 2(c)] the charge density is perfectly uniform, with relatively small fluctuations around $n = 1/2$, for $v_1 = 4$ [see Fig. 2(b)] the evolution starts to have large oscillations between 0 and 1 (here, the two degenerate minima are already developed, but the barriers between them can be easily overcome); eventually, for $v_1 = 7$ [see Fig. 2(a)], ergodicity is broken and the charge density remains stuck in one minimum, since single-electron moves do not allow the system to tunnel easily to the other minimum. We mention that the large Gutzwiller factor used in the calculation prevents the density to be larger than 1 on each site, as it is clear from Fig. 2.

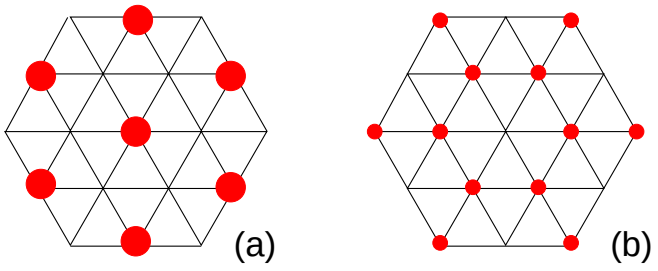

FIG. 3: (Color online) Cartoon picture of the 2−0−0 (a) and 1−1−0 (b) phases that can be stabilized in the triangular lattice at $n = 2/3$ filling, when considering the wave function of Eqs. (19) and (20).

C. Charge-density order in the triangular lattice

Charge-density order can be easily obtained also in two spatial dimensions. As an example, we consider the case of a triangular lattice with $n = 2/3$[20]. We take, similarly to the one-dimensional case, a Slater part in which the lowest-energy levels of a free-fermion Hamiltonian are filled, e.g., $\epsilon(k) = -2[\cos k_x + \cos(k_x/2 + \sqrt{3}k_y/2) + \cos(k_x/2 - \sqrt{3}k_y/2)]$:

$$|\Phi\rangle = \prod_{k<k_F,\sigma} c^{\dagger}_{k,\sigma} |0\rangle. \quad (19)$$

Then, we consider a Jastrow term that contains on-site and nearest-neighbor terms:

$$\mathcal{J} = \exp\left(-g \sum_{i} n_{i,\uparrow} n_{i,\downarrow} - v_1 \sum_{\langle i,j \rangle} n_i n_j \right), \quad (20)$$

where $\langle \dots \rangle$ indicates the nearest-neighbor bonds of the lattice; both g and v_1 are variational parameters that are varied. As for the one-dimensional case discussed before, the variational wave function defined by Eqs. (19) and (20) is suitable for the extended Hubbard model with both on-site U and nearest-neighbor V interactions. In this case, we can describe three different phases: the first one, with small g and v_1, has uniform densities (corresponding to a metal), the second one, with small g and large v_1, develops a charge-density order in which a site with 2 electrons is surrounded by empty sites [denoted by 2−0−0 order; this notation indicates the number of electrons in a triangle; see Fig. 3(a)], and the third one, with large g and small v_1, has another kind of charge-density order in which one empty site is surrounded by singly-occupied sites [denoted by 1−1−0 order; see Fig. 3(b)]. As before, this scenario can be understood from the classical mapping of Eq. (13)[32].

Let us start by considering $g = 0$ and varying the nearest-neighbor parameter v_1. In this way, we can

have a transition between a phase with uniform densities and another phase with 2−0−0 order. In fact, the size scaling of the density-density correlation function (14) for $Q = (4\pi/3, 0)$ [or the symmetry-related one $Q = (2\pi/3, 2\pi/\sqrt{3})$] shows clear evidence of order in the thermodynamic limit for $v_1 \gtrsim 0.4$; see Fig. 4(a). Correspondingly, the local densities on the three sublattices acquire different values when $v_1 \gtrsim 0.4$; see Fig. 4(b).

A richer scenario appears when the Gutzwiller factor g is finite. Indeed, the effect of g is to suppress doubly-occupied sites and, therefore, it acts against the 2−0−0 phase, favoring instead the 1−1−0 order. In Fig. 5, we report the densities on the three sublattices for the case where $g = 5$ and v_1 is varied from 0 to 2.4. The effect of the on-site Jastrow term is clear: on the one hand, it enlarges the stability of the uniform phase, up to $v_1 \simeq 1.2$; on the other hand, it creates an intermediate phase in which two sites have $n_i \approx 1$ and another one has $n_i \approx 0$ (the spatial pattern is such that the empty site is surrounded by occupied sites). Then, for a large enough nearest-neighbor Jastrow parameter, i.e., $v_1 \gtrsim 2$, the 2−0−0 state is obtained again.

D. Orbital order in a two-band model

Let us now turn to a two-band model and show that a simple choice of the Jastrow factor (8) may give rise to orbital order. We focus our attention on the two-dimensional square lattice at half-filling, $n = 2$ (i.e., two electrons per site, each site having two orbitals). The Slater part is constructed from two bands having different width, e.g., $\epsilon_1(k) = -2(\cos k_x + \cos k_y)$ and $\epsilon_2(k) = -(\cos k_x + \cos k_y)$, by filling the lowest-energy states:

$$|\Phi\rangle = \prod_{k<k_F,\alpha,\sigma} c^\dagger_{k,\alpha,\sigma}|0\rangle, \qquad (21)$$

where $\alpha = 1, 2$ indicates the two bands.

The Jastrow factor contains both on-site intra- and inter-orbital terms and the nearest-neighbor intra-orbital term:

$$\mathcal{J} = \exp\left(-\frac{1}{2}\sum_{i,\alpha,\beta} g^{\alpha,\beta} n^\alpha_i n^\beta_i - \sum_{\langle i,j\rangle,\alpha} v_1^{\alpha,\alpha} n^\alpha_i n^\alpha_j\right), \qquad (22)$$

where $\langle \dots \rangle$ indicates the nearest-neighbor bonds of the lattice. In the following, we will fix $g_{1,1} = g_{2,2} = 2$ and $g_{1,2} = g_{2,1} = 1$ and vary $v_1^{1,1} = v_1^{2,2}$. The wave function defined by Eqs. (21) and (22) is suitable to describe the phases of a two-band Hubbard model with both intra-band (U) and inter-band (U') interactions for $U < U'$ and even for $U = U'$ within the paramagnetic sector[33]:

$$\mathcal{H} = -\sum_\alpha t_\alpha \sum_{\langle i,j\rangle,\sigma} c^\dagger_{i,\alpha,\sigma} c_{j,\alpha,\sigma} + \text{h.c.} + U\sum_{i,\alpha} n_{i,\alpha,\uparrow} n_{i,\alpha,\downarrow} + U'\sum_i n_{i,1} n_{i,2}. \qquad (23)$$

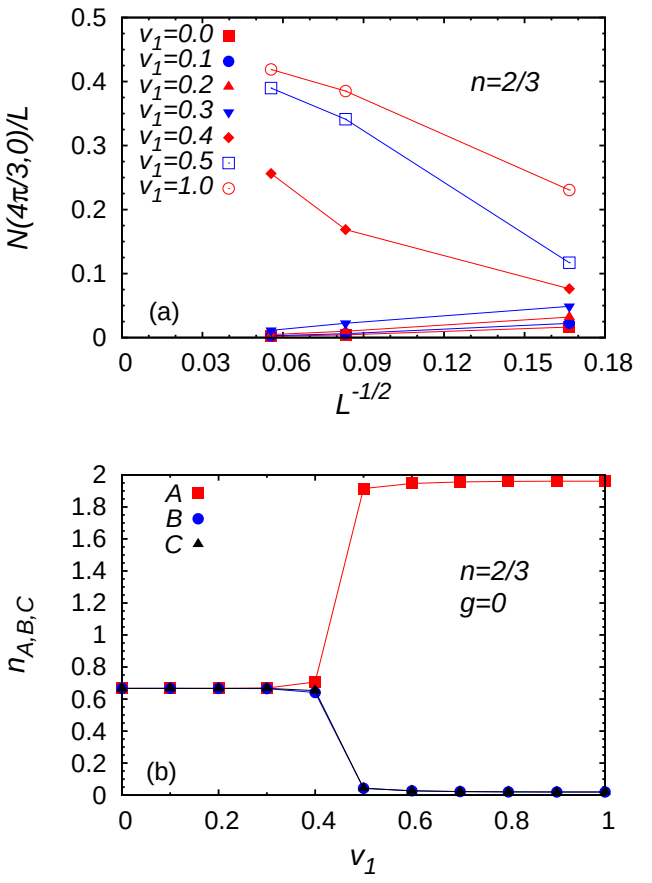

FIG. 4: (Color online) (a) Size scaling of the density-density structure factor $N(Q)/L$ of Eq. (14) at $Q = (4\pi/3, 0)$ for the triangular lattice and filling $n = 2/3$. The variational wave function is given by Eqs. (19) and (20), with $g = 0$ and different values of v_1. (b) Densities of the three sublattices A, B, and C, as a function of the Jastrow parameter v_1, for the same wave function of the upper panel, on a cluster with $L = 324$ sites.

As a function of $v_1^{\alpha,\alpha}$, the wave function describes a transition from a state with uniform densities on each orbital to a state with orbital order, in which the two electrons per site reside on the same orbital (with opposite spin), two neighboring sites having different orbitals occupied; see Fig. 6. This symmetry-broken state can be achieved for a sufficiently large value of $v_1^{\alpha,\alpha}$. In Fig. 7, we show the size scaling of the orbital-resolved density-density structure factor of Eq. (15) for $\alpha = 1$ and $Q = (\pi, \pi)$. For $v_1^{\alpha,\alpha} \lesssim 0.4$, the size scaling clearly indicates that the wave functions has no orbital order, while for $v_1^{\alpha,\alpha} \gtrsim 0.5$, $N^\alpha(Q)/L$ is finite in the thermodynamic limit, implying orbital order.

We finally mention that, as shown in Ref. 33, orbital order can be also favored by the presence of an on-site intra-band pairing; however, here we preferred to consider the simple Slater determinant of Eq. (21) and demonstrate that orbital order can be achieved by the

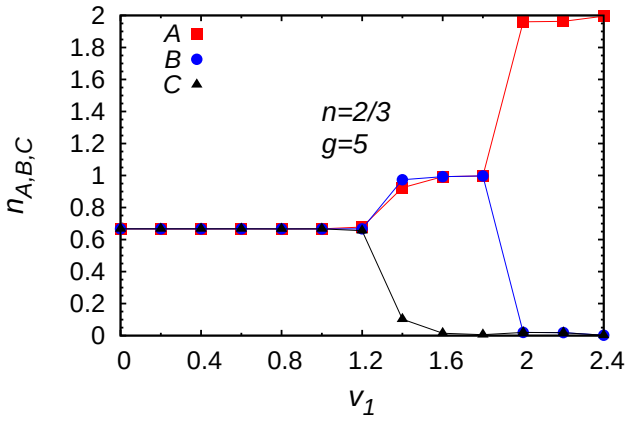

FIG. 5: (Color online) Densities of the three sublattices A, B, and C for the triangular lattice at $n = 2/3$ as a function of the Jastrow parameter v_1, for the variational wave function given by Eqs. (19) and (20) with $g = 5$; the cluster has $L = 324$ sites.

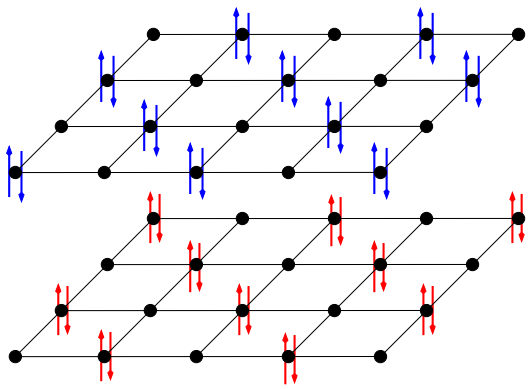

FIG. 6: (Color online) Cartoon picture of the orbital-ordered phase that can be stabilized in the square lattice at $n = 2$ filling, when considering the wave function of Eqs. (21) and (22). The two orbitals are shown as different layers.

Jastrow term (22) only.

III. MAGNETIC AND DIMER ORDERING

A. General concepts and magnetic order

Let us first focus on the possibility of having magnetic long-range order in the fully projected wave function (5). Of course, magnetic order is certainly present whenever the noninteracting state $|\Phi\rangle$ is obtained from an uncorrelated Hamiltonian that *explicitly* contains a magnetic order parameter, thus breaking the spin SU(2) symmetry[34–36]. This is a trivial case that will not be considered here. Instead, we focus on the more interesting case in which $|\Phi\rangle$ has no magnetic order.

Indeed, for certain choices of $|\Phi\rangle$, the Gutzwiller projector of Eq. (4) may generate long-range order. The fully projected wave function may be written in term of a linear superposition of singlet coverings of the lattice[9], the difference with respect to the bosonic LDA state residing upon the actual values of the amplitudes of various singlet coverings. Since, in general, there is not a one-to-one relation between bosonic and fermionic representations of the RVB states[36], it is not *a-priori* obvious that fermionic states may describe magnetically ordered states, as the LDA wave function does.

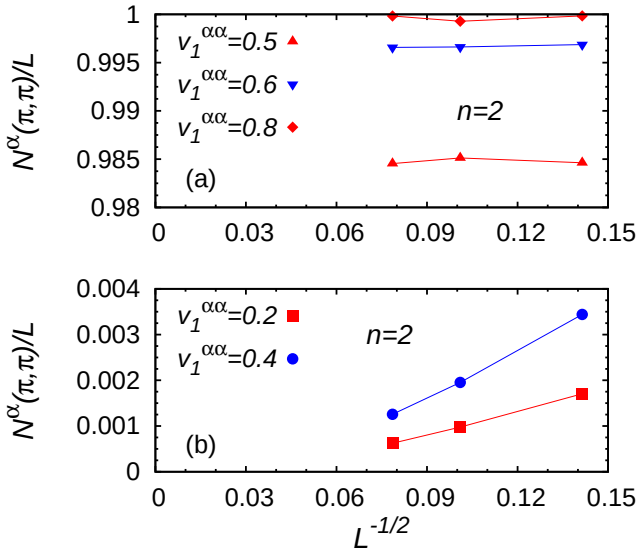

FIG. 7: (Color online) Size scaling of the density-density structure factor $N^\alpha(Q)/L$ of Eq. (15) with $\alpha = 1$ for the two-band model on the square lattice at filling $n = 2$. The variational wave function is given by Eqs. (21) and (22), with $g_{1,1} = g_{2,2} = 2$ and $g_{1,2} = g_{2,1} = 1$. The values of $v_1^{\alpha,\alpha} = 0.5$, 0.6, and 0.8 are shown in (a), while $v_1^{\alpha,\alpha} = 0.2$ and 0.4 are shown in (b).

To have a transparent RVB representation, we use the following parametrization of the noninteracting state[37,38]:

$$|\Phi\rangle = \exp\left(\sum_{i,j} f_{i,j} c^\dagger_{i,\uparrow} c^\dagger_{j,\downarrow}\right)|0\rangle, \qquad (24)$$

which can be obtained as the ground state of a BCS Hamiltonian, containing both pairing and hopping (without performing particle-hole transformations). Here, $c^\dagger_{i,\sigma}$ creates an electron on site i with spin σ. Then, since Eq. (24) does not conserve the number of particles, the correlated state $|\Psi\rangle$ of Eq. (5) must involve a further projection $\mathcal{P}_N$ on the subspace with $N = L$ particles.

In Eq. (24), $f_{i,j}$ is the pair amplitude, which is taken to be symmetric to form singlets in the (i, j) bond:

$$f_{i,j} = f_{j,i}; \qquad (25)$$

in this way, $|\Phi\rangle$ is a total singlet and does not break spin

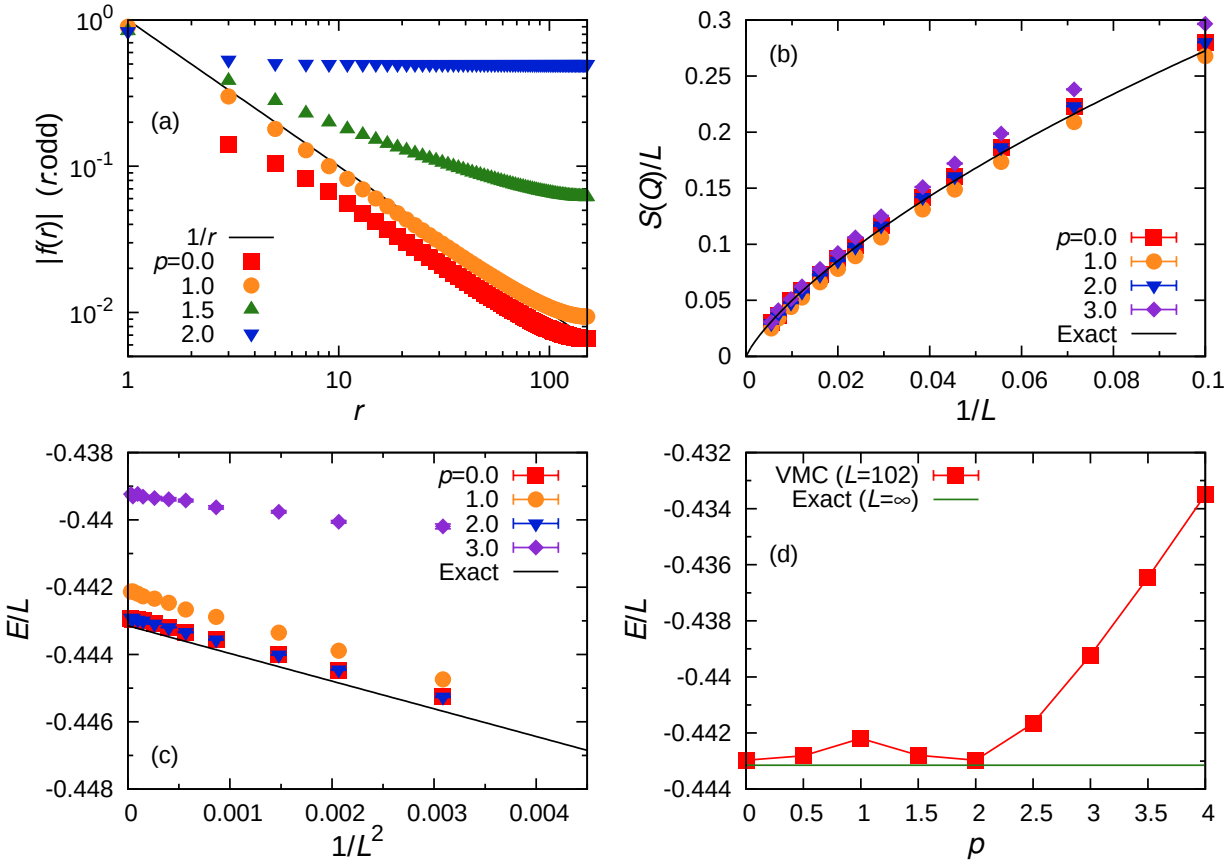

FIG. 8: (Color online) Results for the wave function described by Eqs. (33) and (34) for the one-dimensional lattice. (a) Real-space behavior of the absolute value of the pairing amplitude $f(r)$ as a function of the distance r (for opposite sublattices). (b) Size scaling of the spin-spin structure factor $S(Q)/L$ for $Q = \pi$; the exact (at the leading-order) size scaling for the Heisenberg model is also reported for comparison[39]. (c) Size scaling of the energy per site E/L; the exact (up to order $1/L^2$) size scaling for the Heisenberg model is also reported for comparison[41]. (d) Energy per site E/L versus the parameter p of Eq. (34) for $L = 102$; the exact value of the Heisenberg model for the thermodynamic limit is also reported for comparison.

SU(2) symmetry. Moreover, we consider pairing functions that have all the lattice symmetries. Therefore, as for the LDA wave function, the pairing amplitude $f(r)$ only depends upon the bond length r (bonds with the same r may have different $f(r)$ whenever they are not related by point-group symmetries). The Fourier transform of $f(r)$ is denoted by $f(k)$.

In contrast to charge or orbital order, which are mainly driven by the Jastrow factor (7), the appearance of magnetic order cannot be easily explained through a classical mapping, e.g., Eqs. (12) and (13). Instead, it is mainly due to two circumstances: (i) the presence of the full Gutzwiller projector that enforces no double occupation and (ii) the presence of long-range singlets that create a strong entanglement among spins at very large distances.

Here, we consider one-dimensional chains and the two-dimensional square lattice. Similarly to what has been demonstrated within the bosonic representation of the RVB state, we expect that magnetic order may appear whenever the fully projected state has the Marshall signs and the pairing amplitude decays sufficiently slowly, i.e., $f(r) \propto 1/r^{\alpha}$ with a small α.

Explicitly, we consider a specific parametrization of the pairing amplitude:

$$f(k) = \frac{\Delta(k)}{\epsilon(k) + \sqrt{\epsilon^2(k) + \Delta^2(k)}}, \tag{26}$$

which results from considering $|\Phi\rangle$ as the ground state of the BCS Hamiltonian:

$$\mathcal{H}_{BCS} = \sum_{k,\sigma} \epsilon(k) c^{\dagger}_{k,\sigma} c_{k,\sigma} + \sum_{k} \Delta(k) c^{\dagger}_{k,\uparrow} c^{\dagger}_{-k,\downarrow} + \text{h.c.}, \tag{27}$$

where $c^{\dagger}_{k,\sigma}$ ($c_{k,\sigma}$) creates (destroys) an electron with momentum k and spin σ (along the z axis); $\Delta(k) = \Delta(-k)$ is the singlet pairing amplitude. The BCS spectrum is given by:

$$E(k) = \pm\sqrt{\epsilon^2(k) + \Delta^2(k)}. \tag{28}$$

A gapless (gapped) BCS spectrum $E(k)$ corresponds to a power-law (exponential) decay of the pairing function $f(r)$. Since for the bosonic LDA wave function the existence of magnetic order is related to a sufficiently slow

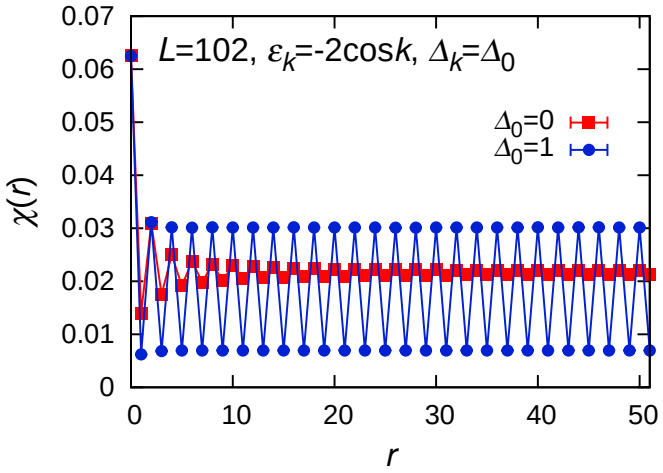

FIG. 9: (Color online) Dimer-dimer correlations of Eq. (39) for the one-dimensional wave function obtained with Eqs. (37) and (38). The gapless case has $\Delta_0 = 0$, while the gapped one has $\Delta_0 = 1$.

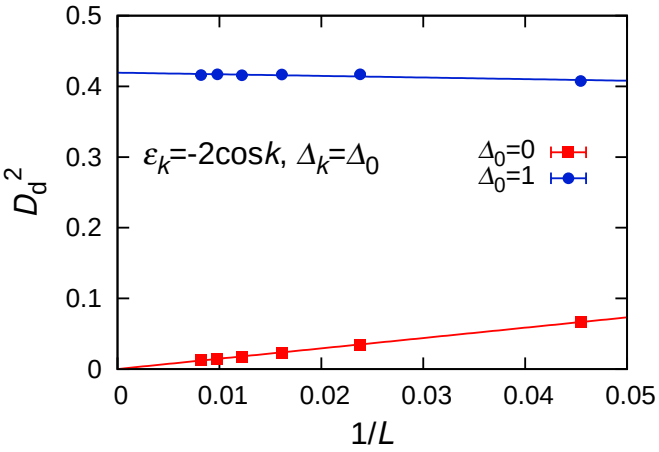

FIG. 10: (Color online) Size scaling of the square of the dimer order parameter of Eq. (40) for the gapless ($\Delta_0 = 0$) and gapped ($\Delta_0 = 1$) cases.

decay of the pairing function, we expect that a gapped BCS spectrum does not give rise to magnetic order.

To fulfill the Marshall sign rule, it is sufficient to take[36]:

$$\epsilon(k+Q) = -\epsilon(k), \tag{29}$$
$$\Delta(k+Q) = -\Delta(k), \tag{30}$$

with $Q = \pi$ in one dimension and $Q = (\pi, \pi)$ for the square lattice. Given the definition of the pairing function (26), we have:

$$f(k+Q) = -\frac{1}{f(k)}. \tag{31}$$

In the following, we will investigate the possibility of having long-range magnetic order with the constraint of Eq. (31) by varying the exponent α of the power-law decay $f(r) \propto 1/r^\alpha$. Magnetic order can be detected by evaluating the spin-spin structure factor:

$$S(q) = \frac{1}{L}\sum_{i,j}\langle \boldsymbol{S}_i \cdot \boldsymbol{S}_j\rangle e^{iq\cdot(r_i - r_j)}; \tag{32}$$

magnetic order with a given pitch vector Q is present whenever the moment (squared) $m^2 = S(Q)/L$ is finite in the thermodynamic limit.

B. RVB wave functions in one dimension

In one spatial dimension (and short-range interactions), antiferromagnetic order is forbidden by the Mermin-Wagner theorem both in the ground state and at finite temperature[17]. Nevertheless, variational wave functions may possess long-range order, as a matter of principle. This is, e.g., the case for bosonic RVB states, as shown in Ref. 18.

In the following, we consider the parametrization (26) with:

$$\epsilon(k) = -2\cos k, \tag{33}$$
$$\Delta(k) = \begin{cases} +|\epsilon(k)|^p & \text{for } \epsilon(k) < 0, \\ -|\epsilon(k)|^p & \text{for } \epsilon(k) > 0, \end{cases} \tag{34}$$

that allows us to easily control the exponent of the power-law decay of $f(r)$. This Ansatz obeys the Marshall sign rule, as clearly seen from Eqs. (29) and (30). We emphasize that this parametrization contains the case of a free Fermi sea (where all states below k_F are occupied while the others are empty) that can be obtained by taking $p = 1$:

$$f(k) = \begin{cases} 1 & \text{for } |k| < k_F, \\ 0 & \text{for } |k| > k_F. \end{cases} \tag{35}$$

Within the parametrization given by Eqs. (33) and (34), we have that the long-range behavior for $f(r)$ is given by $f(r) \propto 1/r^\alpha$, with $\alpha = 1$ for $p \leq 1$, $\alpha = 2 - p$ for $1 \leq p \leq 2$, and $\alpha = 0$ for $p \geq 2$ (the latter case implying that $f(r)$ approaches a constant for large r). In Fig. 8(a), we report the results of the pairing amplitude for different values of p. The spin-spin structure factor shows a peak at $Q = \pi$; however, in all cases, the wave function does not possess magnetic long-range order, in agreement with the Mermin-Wagner theorem, since m vanishes in the thermodynamic limit, as shown in Fig. 8(b). Moreover, also the leading-order corrections in the system size are correct for any value of α, i.e., $S(Q) \propto (\ln cL/2)^{3/2}$, where $c = 25.5$[39].

In the following, we would like to discuss the accuracy of this class of wave functions for the unfrustrated Heisenberg model:

$$\mathcal{H} = J\sum_i \boldsymbol{S}_i \cdot \boldsymbol{S}_{i+1}. \tag{36}$$

It is well known[40] that already the fully projected Fermi sea (35) represents a very good variational ansatz for this model, with an accuracy on the ground-state energy of about 0.2% [i.e., $E/J = -0.44212(1)$ compared with the exact value $E_{ex}/J = 1/4 - \ln 2 = -0.44315$]. Within this class of states, we can strongly improve the accuracy of the fully projected Fermi sea: the best energies are obtained for $p = 0$ [$E/J = -0.44290(1)$] and $p = 2$ [$E/J = -0.44289(1)$]; see Fig. 8(d). In all cases, the finite-size scaling of the energy per site shows the correct behavior in the leading-order corrections (up to order $1/L^2$)[41]; see Fig. 8(c).

C. Dimerization

To conclude the one-dimensional case, we consider the case of dimerization. The possible emergence of valence-bond solids has been discussed in depth for one- and two-dimensional spin models[42]. Few works have used fermionic wave functions that explicitly break the translational symmetry to assess the possible emergence of dimer order in various lattices[43–45]. However, here we are interested in the case where the variational wave function preserves all symmetries, similarly to what has been done in bosonic RVB sates[18]. Indeed, dimer order is present within fermionic RVB wave functions that have short-range pairing amplitudes, as is typical for a gapped BCS spectrum:

$$\epsilon(k) = -2\cos k, \tag{37}$$

$$\Delta(k) = \Delta_0. \tag{38}$$

A gapped BCS spectrum can be obtained for $\Delta_0 > 0$. Similarly, one could consider $\Delta(k) = \Delta_2 \cos(2k)$ (not shown here). Both Δ_0 and Δ_2 are variational parameters. Notice that, in both cases, the Marshall sign rule does not apply, as expected from a generic dimerized phase.

For the dimer-dimer correlation function, one can consider the simplified form that includes only $z-z$ correlations:

$$\chi(r) = \frac{1}{L}\sum_i \langle S^z_i S^z_{i+1} S^z_{i+r} S^z_{i+1+r}\rangle. \tag{39}$$

The order parameter for long-ranged dimerization can then be defined as:

$$D_d^2 = 9 \lim_{r\to\infty} |2\,\chi(r) - \chi(r+1) - \chi(r-1)|, \tag{40}$$

where the factor 9 is introduced in order to take into account the three spin components.

In Fig. 9, we show the dimer-dimer correlations $\chi(r)$ for two cases with $\Delta_0 = 0$ (gapless) and $\Delta_0 = 1$ (gapped). For the former case, $\chi(r) \to$ const for large distances (in the definition of the dimer-dimer correlation, we do not subtract the disconnected terms), indicating that the wave function does not possess any dimer order. By contrast, for the latter case, $\chi(r)$ oscillates between two different values, which is the expected behavior for a dimerized system. We would like to mention that, in presence of a gapped BCS spectrum, both periodic and antiperiodic conditions can be chosen in the BCS Hamiltonian (27), still having a unique ground state. The results shown in Fig. 9 have been obtained with periodic boundary conditions, but a similar outcome can also be obtained with antiperiodic ones. These two states have momentum $k = 0$ and $k = \pi$ and are the ones that become degenerate in the thermodynamic limit[36,46]. The size scaling of the dimer order parameter (40) confirms the possibility of describing a finite dimerization within the class of translationally invariant (gapped) states of Eqs. (37) and (38), as shown in Fig. 10.

D. RVB wave functions in the two-dimensional square lattice

We now discuss the possible emergence of magnetic order in the two-dimensional square lattice. In order to reduce the finite-size effects, we consider 45° degree tilted square lattices, with $L = 2l^2$ sites, l being an odd integer. Similarly to the one-dimensional case, we adopt the following parametrization for the pairing amplitude of Eq. (26):

$$\epsilon(k) = -2(\cos k_x + \cos k_y), \tag{41}$$

$$\Delta(k) = \begin{cases} +|\epsilon(k)|^p & \text{for } \epsilon(k) < 0, \\ -|\epsilon(k)|^p & \text{for } \epsilon(k) > 0. \end{cases} \tag{42}$$

As before, the projected Fermi sea is recovered with $p = 1$. The dominant pairing amplitudes are aligned, in real space, along the diagonals, scaling as $f(r) \propto 1/r^\alpha$, with $\alpha = 2$ for $p \le 1$, $\alpha = 4 - 2p$ for $1 \le p \le 2$, and $\alpha = 0$ for $p \ge 2$. As for the LDA wave function, antiferromagnetic order is expected whenever the pairing function $f(r)$ decays slowly with the distance. Within our parametrization, $\alpha \le 2$, which fulfills this requirement. In Fig. 11(a), we report the pairing function along the diagonal direction for a few values of p. We find that $S(q)$ has a peak at $Q = (\pi, \pi)$. As it was pointed out in the variational Monte Carlo study of Ref. 47, the projected Fermi sea on the square lattice possesses long-range magnetic order. However, in Ref. 47 the actual values of the spin-spin correlations must be corrected by a factor 3/4, given the definition of the isotropic spin-spin correlations. This fact implies that the correct value $m \approx 0.161$ is slightly smaller than the one reported in Ref. 47. Our data are in perfect agreement with $m \approx 0.161$, as shown in Fig. 11(b), for the $p = 1$ case.

Remarkably, long-range magnetic order is obtained for all values of p within the parametrization of Eqs. (41) and (42); see Fig. 11(b). Moreover, the actual values of the finite-size magnetization, as well as its thermodynamic extrapolation, are similar for small and large values of p: for example, we obtain the same values (within a few error bars) for $p = 0$ and $p = 2$. In these cases, the

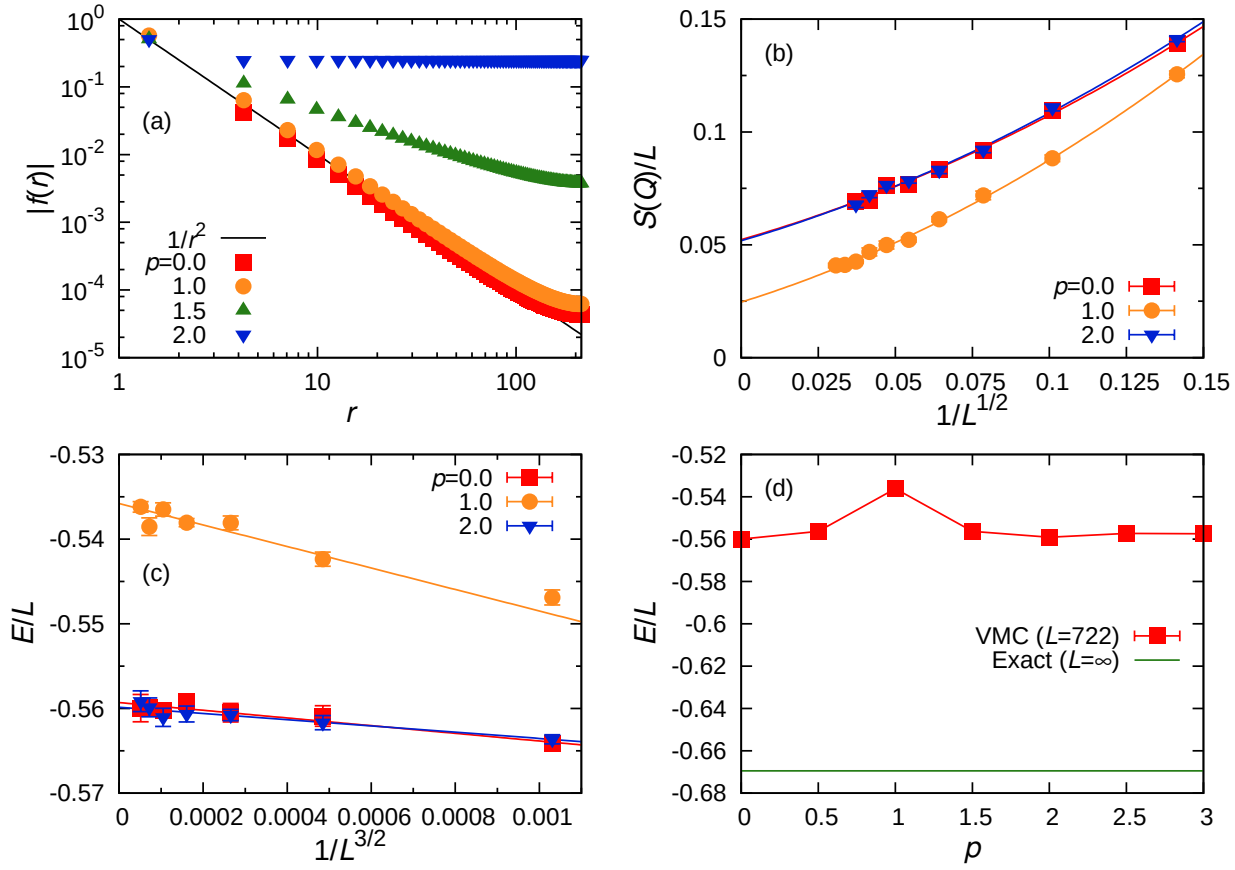

FIG. 11: (Color online) The same as in Fig. 8 but for the two-dimensional case. The variational wave function is described by Eqs. (41) and (42). In (a) $|f(r)|$ is shown along the diagonal direction of the square lattice.

thermodynamic extrapolation gives $m \approx 0.224$, substantially above the value obtained with $p = 1$, but still below the exact value of the unfrustrated Heisenberg model for which $m \approx 0.307$[48–50]. Nevertheless, the fully projected wave function that we have considered here represents a clear example in which it is possible to realize a symmetry breaking within a state that preserves all the symmetries.

Furthermore, in the two-dimensional case the size effects of the energy per site are similar to the ones of two-dimensional ordered antiferromagnets, i.e., with $1/L^{3/2}$ corrections[51,52] [Fig. 11(c)]. However, in this case, the accuracy on the energy is much worse compared to the one-dimensional case, being 16% for the best case[48,49]; see Fig. 11(d).

We conclude this part on the two-dimensional lattice by mentioning that, while fully symmetric wave functions may easily describe situations with collinear magnetic order (we showed the case of Néel order), it is much less trivial to obtain noncollinear magnetic states. Usually, noncollinear orders appears in frustrated lattices, which break the Marshall sign rule. While these states may be easily captured by explicitly breaking the symmetry in the variational wave function[53,54], we could not succeed at reproducing them within a fully symmetric state.

IV. CONCLUSIONS

In this paper, we have shown that Jastrow-Slater wave functions, constructed by applying a Jastrow factor to noninteracting fermionic states, represent a very flexible tool to describe different phases of strongly correlated systems. In particular, it is possible to capture phases with broken symmetries even when these variational states are symmetry-invariant. We reported two classes of examples. In the first one, which applies to itinerant systems (i.e., Hubbard-like models), we showed that charge or orbital order may naturally emerge from a short-range Jastrow factor. The existence of a phase transition and the stabilization of a symmetry-broken phase can be related to a simple mapping between quantum averages and an effective classical partition function, where the strength of the Jastrow factor is directly related to an effective classical temperature. In this case, the configurations that are generated along the Monte Carlo simulation face a breaking of ergodicity, when the Jastrow pseudo-potential is strong enough. This is exactly the same phenomenology of classical systems that undergo phase transitions at low temperatures (e.g., the two-dimensional Ising model).

In the second class, which applies to spin systems (i.e.,

Heisenberg-like models), we have illustrated that antiferromagnetism in two dimensions and dimerization in one dimension may be generated in fully projected wave functions. In this case, there is no classical mapping to guide physical intuition. The emergence of a finite magnetization in two dimensions is due to the presence of the full Gutzwiller projector and of long-range singlets that create a sizable entanglement in the variational wave function, similarly to what happens within the bosonic LDA wave function. In contrast to the previous example on charge/orbital order, in the magnetic order case there is no broken ergodicity in the Monte Carlo single-particle moves (e.g., all the spin components have exactly zero expectation value). This may be ascribed to the fact that the magnetic order is Heisenberg-like while the charge order is Ising-like; the former can easily overcome the potential barrier while the latter cannot. Nevertheless, as for the LDA wave function, a finite magnetization is achieved when singlets are correlated at long distances. We would like to conclude by emphasizing the fact that the presence of the full Gutzwiller projector of Eq. (4) is necessary to obtain magnetic order; otherwise, the soft Gutzwiller term (3) can only change spin-spin correlations at short distances, implying a vanishing magnetization in the thermodynamic limit.

Acknowledgments

We thank S. Sorella for interesting discussions at the early stage of this project. L.F.T. and F.B. acknowledge the support of the Italian Ministry of Education, University, and Research through Grant No. PRIN 2010 2010LLKJBX. R.K., R.V. and C.G acknowledge the support of the German Science Foundation (DFG) through Grant No. SFB/TRR49. The variational Monte Carlo code used for the magnetic calculations is based on a code first developed by D. Tahara. We thank A. Paramekanti for having drawn to our attention Ref. 23. F.B. and R.V. acknowledge the KITP program *New Phases and Emergent Phenomena in Correlated Materials with Strong Spin-Orbit Coupling* and the National Science Foundation (NSF) under Grant No. NSF PHY11-25915.

[1] B. Sutherland, *Beautiful Models* (World Scientific, Singapore, 2004).
[2] J. Bardeen, L.N. Cooper, and J.R. Schrieffer, Phys. Rev. **108**, 1175 (1957).
[3] R.B. Laughlin, Phys. Rev. Lett. **50**, 1395 (1983).
[4] M.C. Gutzwiller, Phys. Rev. Lett. **10**, 159 (1963).
[5] L.F. Tocchio, H. Lee, H.O. Jeschke, R. Valentí, and C. Gros, Phys. Rev. B **87**, 045111 (2013).
[6] J.P.F. LeBlanc, A.E. Antipov, F. Becca, I.W. Bulik, G.K.-L. Chan, C.-M. Chung, Y. Deng, M. Ferrero, T.M. Henderson, C.A. Jiménez-Hoyos, E. Kozik, X.-W. Liu, A.J. Millis, N.V. Prokof'ev, M. Qin, G.E. Scuseria, H. Shi, B.V. Svistunov, L.F. Tocchio, I.S. Tupitsyn, S.R. White, S. Zhang, B.-X. Zheng, Z. Zhu, and E. Gull, Phys. Rev. X **5**, 041041 (2015).
[7] S. Sorella and E. Tosatti, Europhys. Lett. **19**, 699 (1992).
[8] S. Liang, B. Doucot, and P.W. Anderson, Phys. Rev. Lett. **61**, 365 (1988).
[9] P.W. Anderson, Science **235**, 1196 (1987); Mater. Res. Bull. **8**, 153 (1973).
[10] K.S.D. Beach, arXiv:0707.0297.
[11] W. Marshall, Proc. R. Soc. (London), Ser. A **232**, 48 (1955).
[12] P. Sindzingre, P. Lecheminant, and C. Lhuillier, Phys. Rev. B **50**, 3108 (1994).
[13] H. Yokoyama and H. Shiba, J. Phys. Soc. Jpn. **56**, 1490 (1987).
[14] H. Yokoyama and H. Shiba, J. Phys. Soc. Jpn. **56**, 3582 (1987).
[15] C. Gros, Ann. Phys. (N.Y.) **189**, 53 (1989).
[16] M. Capello, F. Becca, M. Fabrizio, S. Sorella, and E. Tosatti, Phys. Rev. Lett. **94**, 026406 (2005).
[17] L. Pitaevskii and S. Stringari, J. Low Temp. Phys. **85**, 377 (1991).
[18] Y.-C. Lin, Y. Tang, J. Lou, and A.W. Sandvik, Phys. Rev. B **86**, 144405 (2012).
[19] E.H. Lieb, T.D. Schultz, D.C. Mattis, Ann. Phys. (N.Y.) **16**, 407 (1961).
[20] H. Watanabe and M. Ogata, J. Phys. Soc. Jpn. **74**, 2901 (2005).
[21] M. Miyazaki, C. Hotta, S. Miyahara, K. Matsuda, and N. Furukawa, J. Phys. Soc. Jpn. **78**, 014707 (2009).
[22] L.F. Tocchio, C. Gros, X.-F. Zhang, and S. Eggert, Phys. Rev. Lett. **113**, 246405 (2014).
[23] O.I. Motrunich and P.A. Lee, Phys. Rev. B **69**, 214516 (2004).
[24] M. Capello, F. Becca, S. Yunoki, and S. Sorella, Phys. Rev. B **73**, 245116 (2006).
[25] M. Capello, F. Becca, M. Fabrizio, and S. Sorella, Phys. Rev. B **77**, 144517 (2008).
[26] F. Mila and X. Zotos, Europhys. Lett. **24**, 133 (1993).
[27] K. Penc and F. Mila, Phys. Rev. B **49**, 9670 (1994).
[28] H. Yoshioka, M. Tsuchiizu, and Y. Suzumura, J. Phys. Soc. Jpn. **69**, 651 (2000).
[29] K. Sano and Y. Ōno, Phys. Rev. B **70**, 155102 (2004).
[30] S. Ejima, F. Gebhard, and S. Nishimoto, Europhys. Lett. **70**, 492 (2005).
[31] T. Shirakawa and E. Jeckelmann, Phys. Rev. B **79**, 195121 (2009).
[32] The same quantum-to-classical mapping for $n = 1/3$ has been discussed in Ref. 23 in the context of charge order in Na_xCoO_2.
[33] L.F. Tocchio, F. Arrigoni, S. Sorella, and F. Becca, J. Phys.: Condens. Matter **28**, 105602 (2016).
[34] H. Yokoyama and H. Shiba, J. Phys. Soc. Jpn. **56**, 3570 (1987).
[35] G.J. Chen, R.J. Joynt, F.C. Zhang, and C. Gros, Phys. Rev. B **42**, 2662 (1990).
[36] F. Becca, L. Capriotti, A. Parola, and S. Sorella, *Variational Wave Functions for Frustrated Magnetic Models*,

Springer Series in Solid-State Sciences, edited by Claudine Lacroix, Philippe Mendels, and Frederic Mila, Vol. 164 (Springer, Berlin, Heidelberg, 2011), p. 379.
[37] A. Himeda and M. Ogata, Phys. Rev. Lett. **85**, 4345 (2000).
[38] D. Tahara and M. Imada, J. Phys. Soc. Jpn. **77**, 114701 (2008).
[39] K.A. Hallberg, P. Horsch, and G. Martinez, Phys. Rev. B **52**, 719(R) (1995).
[40] C. Gros, R. Joynt, and T.M. Rice, Phys. Rev. B **36**, 381 (1987).
[41] I. Affleck, Phys. Rev. Lett. **56**, 746 (1986).
[42] N. Read and S. Sachdev, Phys. Rev. Lett. **62**, 1694 (1989); Phys. Rev. B **42**, 4568 (1990).
[43] D. Heidarian, S. Sorella, and F. Becca, Phys. Rev. B **80**, 012404 (2009).
[44] Y. Iqbal, F. Becca, and D. Poilblanc, Phys. Rev. B **83**, 100404 (2011).
[45] S. Morita, R. Kaneko, and M. Imada, J. Phys. Soc. Jpn. **84**, 024720 (2015).
[46] S. Sorella, L. Capriotti, F. Becca, and A. Parola, Phys. Rev. Lett. **91**, 257005 (2003).
[47] T. Li, Europhys. Lett. **103**, 57002 (2013).
[48] A.W. Sandvik, Phys. Rev. B **56**, 11678 (1997).
[49] M. Calandra Buonaura and S. Sorella, Phys. Rev. B **57**, 11446 (1998).
[50] F.-J. Jiang and U.-J. Wiese, Phys. Rev. B **83**, 155120 (2011).
[51] H. Neuberger and T. Ziman, Phys. Rev. B **39**, 2608 (1989).
[52] D.S. Fisher, Phys. Rev. B **39**, 11783 (1989).
[53] L.F. Tocchio, H. Feldner, F. Becca, R. Valentí, and C. Gros, Phys. Rev. B **87**, 035143 (2013).
[54] E. Ghorbani, L.F. Tocchio, and F. Becca, Phys. Rev. B **93**, 085111 (2016).